Propellants,
Explosives,
Pyrotechnics

Full Paper

Characterization of a Series of Nitrogen-Rich Molecules using Laser Induced Breakdown Spectroscopy

Frank C. De Lucia, Jr.*, Jennifer L. Gottfried

United States Army Research Laboratory, Aberdeen Pround, MD, 21005 (USA)

Received: January 13, 2010; revised version: February 08, 2010

DOI: 10.1002/prep.201000009

Abstract

A series of nitrogen-rich molecules, such as 5-aminotetrazolium nitrate (HAT-NO_3) and hydrazinebistetrazole (HBT), bis(2,2,2-trinitroethyl)-hydrazodicarboxylate (BTHC), cyclotrimethylene trinitramine (RDX), trinitrotoluene (TNT), melamine, sucrose, and L-glutamine were studied using laser-induced breakdown spectroscopy (LIBS). The atomic emission intensities and intensity ratios of the constituent elements from the LIBS spectrum were shown to correlate with the mole fractions and stoichiometries of the molecules. In addition, the amount of oxygen present in the molecule influenced the emission intensities of molecular fragments such as C_2. Finally, we used principal components analysis to analyze the data from the LIBS spectra and separate the different organic molecules based on the atomic emission intensities and ratios.

Keywords: Energetic Materials, Emission Spectroscopy, LIBS, Plasma Chemistry

1 Introduction

New classes of high-energy, high-density materials (HEDM) are being studied for possible use as environmentally friendly or "green" energetic materials [1, 2]. While conventional military explosives such as cyclotrimethylene trinitramine (RDX) and trinitrotoluene (TNT) derive most of their energy from oxidation of the carbon backbone, high-nitrogen compounds, such as aminotetrazole and nitrotetrazole derivatives containing up to 85% nitrogen content, derive most of their energy from their very high positive heats of formation [3]. Many of these promising compounds have been synthesized and show the desired insensitivity to electrostatic discharge, friction, and impact while having very high explosive powers. Spectroscopic methods such as Raman and IR spectroscopy, NMR, and X-ray crystallography have been used in the characterization of these materials to elucidate their molecular structures. Here, we have used laser-induced breakdown spectroscopy (LIBS) to investigate a series of nitrogen-rich, low carbon content compounds that have been synthesized and studied for use in possible military applications.

LIBS is a spectroscopic analysis technique that uses the light emitted from a laser-generated microplasma to determine the composition of the sample on the basis of elemental and molecular emission intensities [4]. The ability of LIBS to provide rapid, multi-element microanalysis of bulk samples (solid, liquid, gas, and aerosol) in the parts-per-million range with little or no sample preparation has been widely demonstrated [5 – 12]. LIBS holds particular promise for the detection and identification of explosives because of its intrinsic capability for minimally destructive, in situ, real-time detection and analysis of a broad range of chemical species [13].

The ability of LIBS to discriminate materials with similar stoichiometry has been demonstrated with liquid nerve agent simulants [14] and solid organic (non-explosive) materials [15]. At the US Army Research Laboratory, we have used LIBS to characterize organic military explosives such as RDX and TNT by tracking the relative amount of oxygen and nitrogen (the oxidizers) compared to carbon and hydrogen (fuel components) using the atomic emission intensities [16 – 18]. In general, the oxidizer-to-fuel atomic emission ratios are higher for explosives because of the higher oxygen and nitrogen density (usually due to an oxide of nitrogen) compared to non-explosives. We have discriminated RDX, TNT, and composition-B (63% RDX, 36% TNT, 1% wax) from numerous non-explosive organic and inorganic interferents on a variety of substrates [19, 20]. A more detailed study using a wide array of explosive organic molecules for LIBS characterization would provide more information about the relationship between the emission from the microplasma and the chemical composition of the target material, and may also provide some information about the chemical reactions occurring in the high-temperature plasma environment ($\sim$12 000 K).

* Corresponding author; e-mail: fdelucia@arl.army.mil

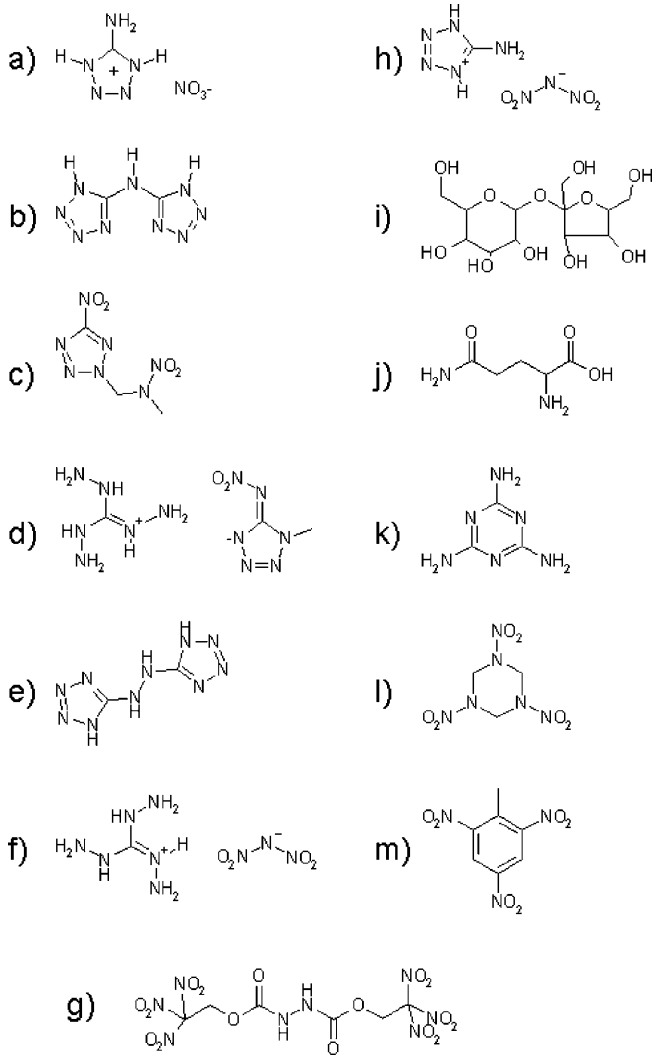

Figure 1. Molecular structures of organic compounds: a) HAT-NO_3, b) H_2bta, c) NTNAP, d) TAG-1 MeAtNO_2, e) HBT, f) TAG-DN, g) BTHC, h) HAT-DN, i) sucrose, j) L-glutamine, k) melamine, l) RDX, and m) TNT.

For the present study, we used LIBS to track the emission from the constituent elements of 13 organic compounds, including seven nitrogen-rich compounds [21 – 28], bis(2,2,2-trinitroethyl)-hydrazodicarboxylate (BTHC) [29], RDX, TNT, and three non-explosives (L-glutamine, sucrose, and melamine). The structures, nomenclature, and the molecular formula of the 13 compounds are displayed in Figure 1 and Table 1. We collected and characterized LIBS spectra from each material. We used carbon, hydrogen, nitrogen, and oxygen atomic emission lines to calculate atomic emission ratios and correlate them to the stoichiometric ratios. In contrast to Tran et al. [15], who measured different ratios for each compound, the six atomic emission ratios of interest to us (N/C, O/C, H/C, O/H, N/H, and O/N) were obtained for each of the 13 compounds simultaneously (along with other spectral features). Also in contrast to [15], the samples were prepared in a heterogeneous manner in order to observe how well LIBS can track the stoichiometry even when the laser/sample interaction varies considerably from shot to shot. The wide range of stoichiometries offered by the nitrogen-rich compounds allowed us to observe how the LIBS atomic and molecular emissions were influenced by chemical composition. We also observed trends in molecular fragment emission that were dependent on the chemical composition of the sample.

2 Experimental Part

The seven high-nitrogen compounds, BTHC, RDX, and TNT were provided by ARL colleagues. Melamine and L-glutamine were acquired from Sigma Aldrich. The sucrose was from standard granulated sugar. A small amount of each sample ($\sim$1 mg) was deposited onto aluminum foil substrates. The samples were crushed by a Teflon block covered in aluminum foil and spread/smeared across the surface of the aluminum. The coverage was heterogeneous and aluminum could be seen through the thin layer of sample. A Nd:YAG laser (Big Sky, CFR400, $\sim$115 mJ) was used as the laser source for the LIBS setup and was focused by a 10 cm focal length lens onto the sample surface and fired in a single-shot mode. The emission from the resulting microplasma was collected by a parabolic mirror and focused onto a seven-fiber (600 μm diameter) bundle. Each fiber was

Table 1. LIBS spectra of the following 13 organic molecules were collected for analysis.

Sample name	Nomenclature	Molecular formula	No. of spectra
5-Aminotetrazolium nitrate [21]	HAT-NO_3	$CH_4N_6O_3$	129
Biz(tetrazolyl)amine [22]	H_2bta	$C_2H_3N_9$	132
1-Nitrotetrazolato-2-nitro-2-aza-propane [23]	NTNAP	$C_3H_6N_7O_4$	138
Triaminoguanidinium-1-methyl-5-nitriminotetrazolate [24, 25]	TAG-1 MeAtNO_2	$C_3H_{12}N_{12}O_2$	136
Hydrazinebistetrazole [26]	HBT	$C_2H_4N_{10}$	142
1,3,5,-Triaminoguanidinium dinitramide [27]	TAG-DN	$CH_9N_9O_4$	33
Bis(2,2,2-trinitroethyl)-hydrazodicarboxylate [29]	BTHC	$C_6H_6N_8O_{16}$	37
5-Aminotetrazolium dinitramide [28]	HAT-DN	$CH_4N_8O_4$	41
Cyclotrimethylene trinitramine	RDX	$C_3H_6N_6O_6$	76
Trinitrotoluene	TNT	$C_7H_5N_3O_6$	62
Melamine	Melamine	$C_3H_6N_6$	160
L-glutamine	L-Glutamine	$C_5H_{10}N_2O_3$	91
Sucrose	Sucrose	$C_{12}H_{22}O_{11}$	67

connected to one of the seven channels in the multi-channel CCD spectrometer (Ocean Optics Inc., LIBS 2500+), giving broadband coverage from 200–950 nm at relatively high resolution (~0.1 nm). The spectrometer was set to begin collecting light 1.25 μs after the plasma initiation in order to reduce the background continuum. The spectrometer gate width was 1 ms. An argon flow was directed across the sample surface where the microplasma was formed in order to reduce the atmospheric interference from nitrogen and oxygen.

Single-shot LIBS spectra were collected from each sample type. An initial series of spectra were collected from each compound. For six of the compounds (HAT-NO_3, H_2bta, NTNAP, TAG-1 MeAtNO_2, HBT, and melamine), an additional series of spectra were collected several days later on the same samples that had been stored open to the atmosphere. The total number of laser shots for each sample varies because not all the spectra were used for the analysis. We kept ~80% of each of the 13 sample sets based on those with the highest carbon background-corrected intensity. The total number of spectra used in the analysis for each sample is listed in Table 1. Due to the heterogeneous nature of the sample coverage, the laser interacted with different amounts of material for each laser shot. The large relative standard deviation (RSD) of the carbon intensity peak at 247 nm reflects the heterogeneity of the sample. For example, the RSD for carbon atomic emission intensity in melamine and NTNAP is 28 and 24%, respectively. Typically the RSD of LIBS emission intensities for bulk samples is around 5–10%.

In Table 2, the range of stoichiometric ratios and mole fractions covered by the 13 organic compounds are shown. Atomic emission ratios corresponding to the stoichiometric ratios in Table 2 were calculated as follows. The peak intensities of multiple atomic emission lines of carbon and nitrogen (listed in Table 3) were background-subtracted and then summed. Although multiple oxygen lines were observed in the spectra, only the background-subtracted 777 nm emission line was used in the analysis since the presence of residual atmospheric oxygen resulted in non-zero summed oxygen intensities when multiple lines were used in samples without oxygen. For some of the single-shot spectra the intensity of the hydrogen line at 656 nm saturated the detector. Instead of using the peak intensity, a point on the shoulder of the hydrogen emission line at 656 nm was used and background-subtracted. We could not use the hydrogen emission at ~485 nm because of interference from argon emission lines and AlO molecular emission in some samples. We calculated the six stoichiometric ratios for each compound studied using the summed carbon and nitrogen background-corrected intensities, the oxygen background-corrected peak emission intensity, and the hydrogen background-corrected shoulder emission intensity. In addition, the total carbon, hydrogen, nitrogen, and oxygen intensities were normalized to the summed intensity of the four elements.

An average was calculated for each atomic emission ratio for each sample. We graphed the atomic emission ratios and the normalized intensities against the stoichiometric ratios of each compound and the mole fraction of each element, respectively. A linear function was used to fit the data points. The Pearson correlation coefficient (r) was calculated for each curve fit. The r value was used as a measure of the correlation between the atomic emission ratios and the stoichiometric ratios. Confidence bands and prediction bands were calculated from the uncertainty of the linear model fit. The confidence band is where the linear fit will fall 95% of the time if the experiment is repeated for numerous iterations. The prediction band shows where 95% of the measured points should fall. Principal components analysis (PCA) can be used to reduce a complex data set and extract useful information that describes major trends in the data. We used PCA to demonstrate how the samples can be separated based on their normalized intensities and atomic emission intensities.

Table 2. Stoichiometric and mole fraction ranges in the 13 molecules listed from Table 1.

	Stoichiometric ratio range		Mole fraction range (%)
N/C	0–9	Carbon	4–33
N/H	0–3	Hydrogen	17–50
O/C	0–4	Nitrogen	0–64
O/H	0–2.67	Oxygen	0–44
O/N	0–2		
H/C	0–9		

Table 3. Atomic emission lines for carbon and nitrogen used for analysis of stoichiometries and mole fractions

Carbon atomic lines (nm)	Nitrogen atomic lines (nm)		
247	742	856	871.8
833	744	859	872
906	746	862	874
907	818.4	865	903
908	818.8	868	904.5
909	821	868.3	904.9
911	821.6	870	938
940	824	871	939

3 Results

We collected LIBS spectra under argon from residues of all the samples listed in Table 1 and the blank aluminum substrate. First, we determined the atomic emission peaks that originated from the argon bath gas and the aluminum substrate. Argon lines occur at 697, 707, 750, 764, 795, 801, 810, 826, 842, 852, and 912 nm. Aluminum emission lines are at 227, 237, 258, 308, 309, 394, and 396 nm. Next, for each sample, we identified all of the emission peaks associated with the residue. In Figure 2, a LIBS spectrum of the HAT-NO_3 spectra is displayed with a LIBS spectrum of the blank aluminum substrate. Several key elements are highlighted in

the insets including carbon, hydrogen, oxygen, nitrogen, calcium, potassium, and CN and AlO molecular emissions.

The small oxygen emission observed in the aluminum blank is probably due to oxygen already present on the aluminum surface. When a second LIBS spectrum is obtained from the same spot on the aluminum blank as the first spectrum, i.e. a cleaning shot is fired first; the oxygen emission at 777 nm is no longer present. We also observed sodium and C_2 molecular emission in some of the samples. In Figure 3, LIBS spectra of H_2bta, sucrose, and blank aluminum are shown.

The H_2bta molecule does not contain any oxygen and the sucrose does not contain any nitrogen, so there is no atomic emission due to nitrogen in the latter and oxygen in the former. C_2 molecular emission at 516.5 nm and sodium emission at 589 nm are observed in both spectra. LIBS spectra from a high nitrogen molecule (TAG-1 $MeAtNO_2$), a conventional explosive (RDX), and a nitrogen-containing hydrocarbon (melamine) are shown in Figure 4. Some of the atomic and molecular emission peaks due to the molecules are labeled.

A zoomed in view of the spectra shows that the oxygen intensity is greater for RDX then TAG-1 $MeAtNO_2$ and that there is minimal if any oxygen emission from the melamine as expected, since the oxygen mole fraction in the RDX, the TAG-1 $MeAtNO_2$, and the melamine is 29, 7, and 0%, respectively. In Figure 5, we show the correlation of the normalized atomic emission intensities of carbon, hydrogen, nitrogen, and oxygen from each of 13 compounds with the mole fraction of each of the constituent elements for each compound. The correlation coefficient r was calculated for each element, as were the confidence and prediction bands.

The r value is greater than 0.9 for each element, indicating a strong correlation between the normalized intensity and the mole fraction. The hydrogen correlation graph has the lowest r value and this can be attributed to using the shoulder on the 656 nm emission peak due to the saturation of the peak intensity, since changes in both the line profile (due to changing plasma conditions) and the peak intensity are reflected in the shoulder intensity at a particular point. Next, we calculated six atomic emission ratios for each compound (O/C, N/C, H/C, N/H, O/H, and O/N) using the normalized emission intensities. The six correlation graphs of each atomic emission ratio against the stoichiometric ratio for each compound are displayed in Figure 6.

Again the r value is greater than 0.9 for each ratio, indicating a strong correlation between the atomic emission ratios and the actual chemical composition of each compound. In general, the correlation between the emission intensity ratios and the stoichiometric ratios is stronger than the correlation between the peak emission intensities and mole fractions. The use of summed intensity ratios minimizes the effect of shot-to-shot variations in the plasma temperature due to laser power fluctuations and sample

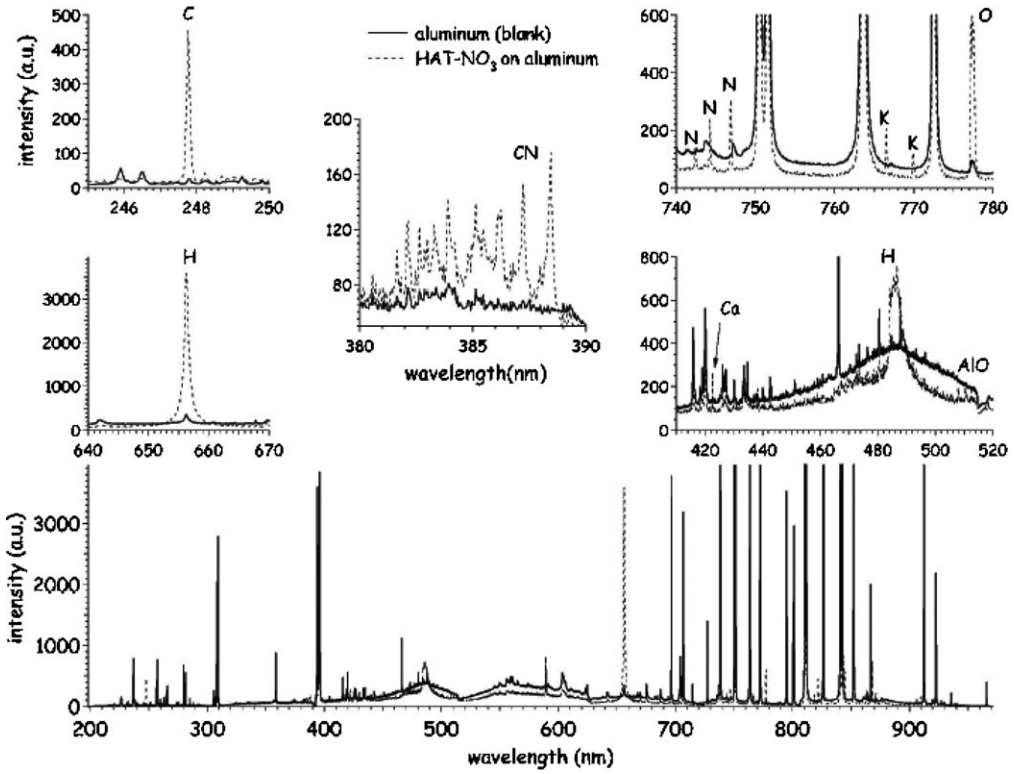

Figure 2. Broadband LIBS spectra (bottom) of aluminum and HAT-NO_3 on aluminum. Insets focus on regions of interest in the LIBS spectra that display carbon, hydrogen, nitrogen, oxygen, potassium, and calcium atomic emission as well as CN and AlO molecular emission.

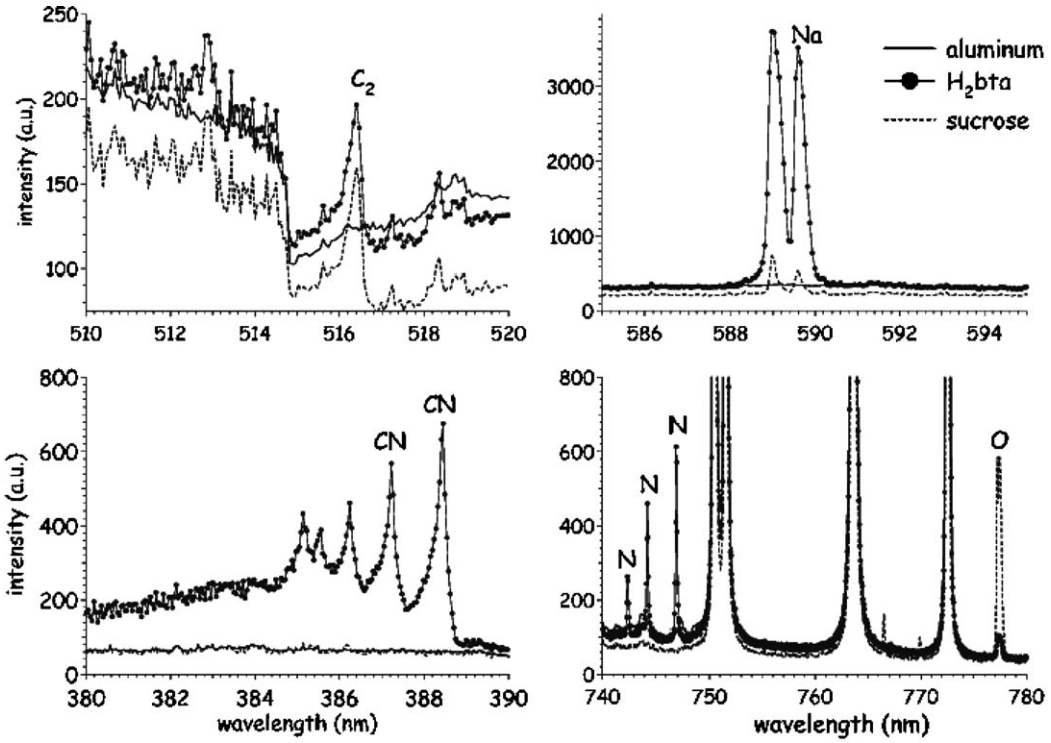

Figure 3. Different LIBS spectral regions of aluminum, H_2bta, and sucrose that compare molecular and atomic emission of C_2, CN, sodium, nitrogen, and oxygen.

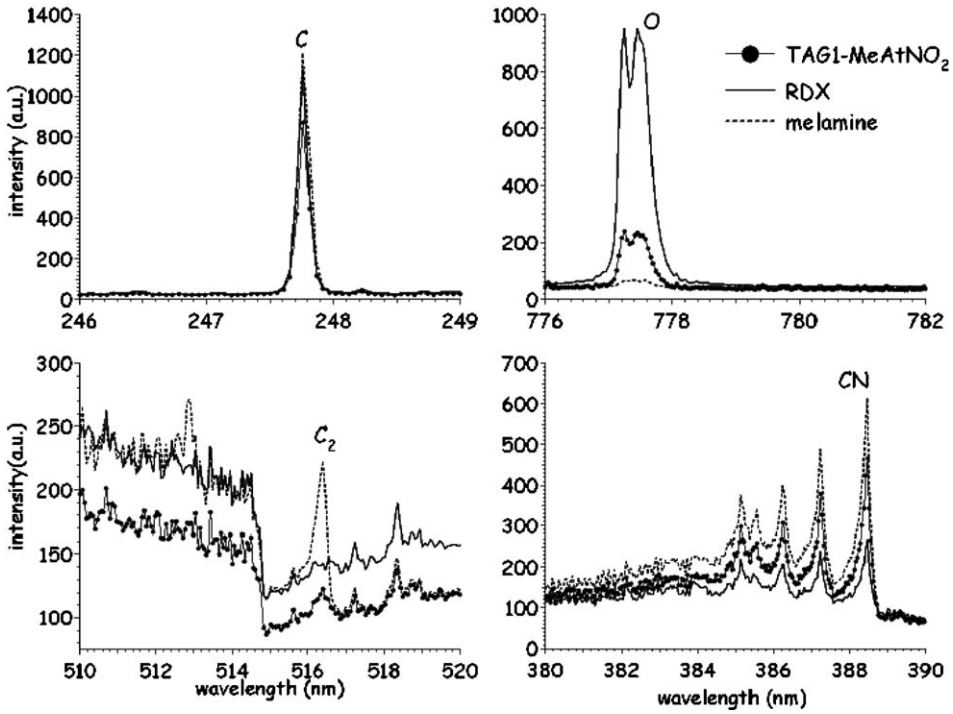

Figure 4. LIBS spectral regions that compare atomic and molecular emission of carbon, oxygen, C_2, and CN from TAG1-MeAtNO$_2$, RDX, and melamine Description of figure 1.

inhomogeneity and provides a method for discriminating between materials with the same elemental constituents [20].

In addition to the atomic emission, we observed molecular emission from CN, C_2, and AlO in some of the compounds. In air, CN is formed by recombination of C_2

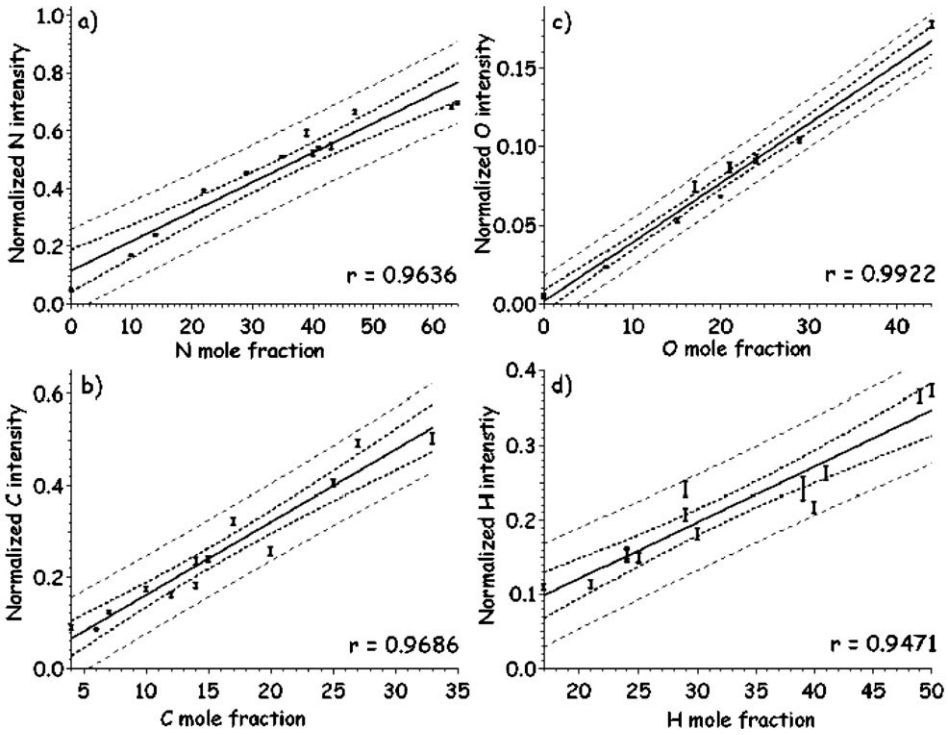

Figure 5. Correlation graphs of normalized atomic emission intensities against the corresponding mole fraction of the constituent elements of the 13 organic compounds a) nitrogen, b) carbon, c) oxygen, and d) hydrogen.

with atmospheric nitrogen [30]. In the argon bath gas, however, the formation of CN must be due to the carbon and nitrogen from the molecule. Therefore there is no CN emission in the LIBS spectrum of sucrose. In Figure 7a, we graphed a contour plot of the carbon and nitrogen mole fraction against the CN emission intensity of each compound. As the mole fraction of C and N increase so does the CN emission intensity, as expected. When the mole fraction of carbon and nitrogen is graphed with the atomic carbon emission intensity at 247 nm in Figure 7b, we observe that the atomic emission intensity decreases as the nitrogen mole fraction increases.

The decrease is presumably due to increased CN formation. Possible reaction pathways are shown below [31].

$$C + N + M \rightarrow CN + M \quad (1)$$

$$C_2 + N_2 \rightarrow 2CN \quad (2)$$

$$C + N_2 \rightarrow CN + N \quad (3)$$

In Figure 7a, we see the dependence of CN molecular emission on the mole fraction of carbon. However, we do not observe the same dependence of CN molecular emission from the amount of C_2 molecular emission (Figure 7c) suggesting that reaction (1) and (3) are the most likely pathways for CN formation under argon with these samples.

The carbon that forms C_2 must originate from the compound. However, we do not observe C_2 emission in the LIBS spectrum of each compound, even though they all contain carbon. In addition, the C_2 emission intensity does not directly correlate with the mole fraction of carbon ($r = 0.4711$). The other constituent elements could have an effect on the C_2 emission intensity. When we graphed the carbon and oxygen mole fraction with the C_2 emission intensity in Figure 7d, we observed that the C_2 emission increases as the carbon mole fraction increases, but C_2 emission decreases as the oxygen mole fraction increases. Song et al. observed that an oxygen-poor environment leads to higher C_2 emission in an RDX-aluminum nanopowder combustion [32]. The following reactions are possible pathways for the observed behavior of the C_2 emission in the presence of oxygen [31].

$$C_2 + O \rightarrow CO + C \quad (4)$$

$$C_2 + O_2 \rightarrow CO + CO \quad (5)$$

The only substantial oxygen present in the plasma in an argon atmosphere is from the residue (trace amounts of oxygen may be present on the substrate surface or in the argon gas). RDX and melamine have almost identical stoichiometries except for the oxygen present in RDX. As expected, C_2 emission is observed in the LIBS spectrum of melamine, while no C_2 emission is observed in the LIBS spectrum of RDX (Figure 4). We also observe C_2 emission in the LIBS spectrum of H_2bta since the compound does not contain oxygen (Figure 3). However, if the LIBS spectrum is collected in air instead of argon, there is no C_2 emission as seen in Figure 8. The oxygen mole fraction has minimal

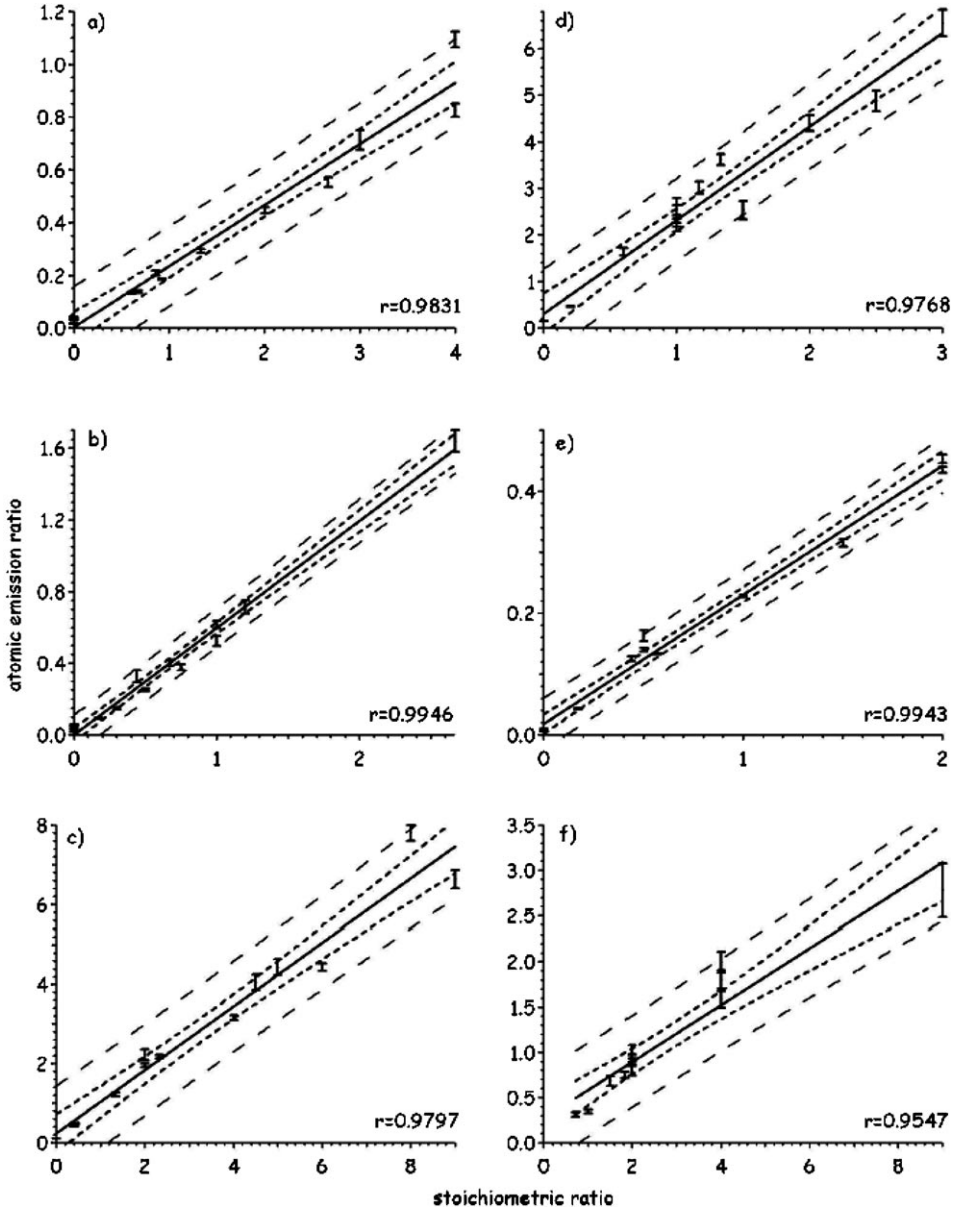

Figure 6. Correlation graphs of six atomic emission ratios against the corresponding stoichiometric ratios of the 13 organic compounds a) O/C, b) O/H, c) N/C, d) N/H, e) O/N, and f) H/C.

effect on the atomic carbon emission intensity at 247 nm as seen in Figure 7e, so the oxygen must react with the carbon after the C_2 formation in order to prevent C_2 emission.

Aluminum oxide molecular emission was not observed on the blank aluminum. Residual oxygen on the surface of the aluminum was not sufficient to generate AlO emission in the argon environment. Thus, the oxygen that forms AlO must originate from the organic residues. However, the AlO molecular emission did not linearly correlate with the oxygen mole fraction. When the AlO emission intensity is graphed against the oxygen and carbon mole fraction in Figure 7f the AlO emission intensity increases as the oxygen mole fraction increases for low carbon mole fractions. The reactions (4) and (5) are possible pathways for the oxygen to be scavenged by carbon thus reducing the AlO formation and subsequent emission.

Based on the prediction bands generated by the various correlation graphs, one particular normalized intensity, atomic emission ratio, or molecular emission intensity are not enough to predict the exact stoichiometric ratio or mole fraction of a compound. However, all six atomic emission ratios and the normalized intensities could be used as inputs into more advanced chemometric analysis to separate the different compounds and ultimately identify the actual stochiometries and mole fractions. We used a combination of 14 atomic emission ratios, normalized intensities, and linear combinations of the normalized intensities as inputs for a PCA model. The first three principal components

Propellants,
Explosives,
Pyrotechnics

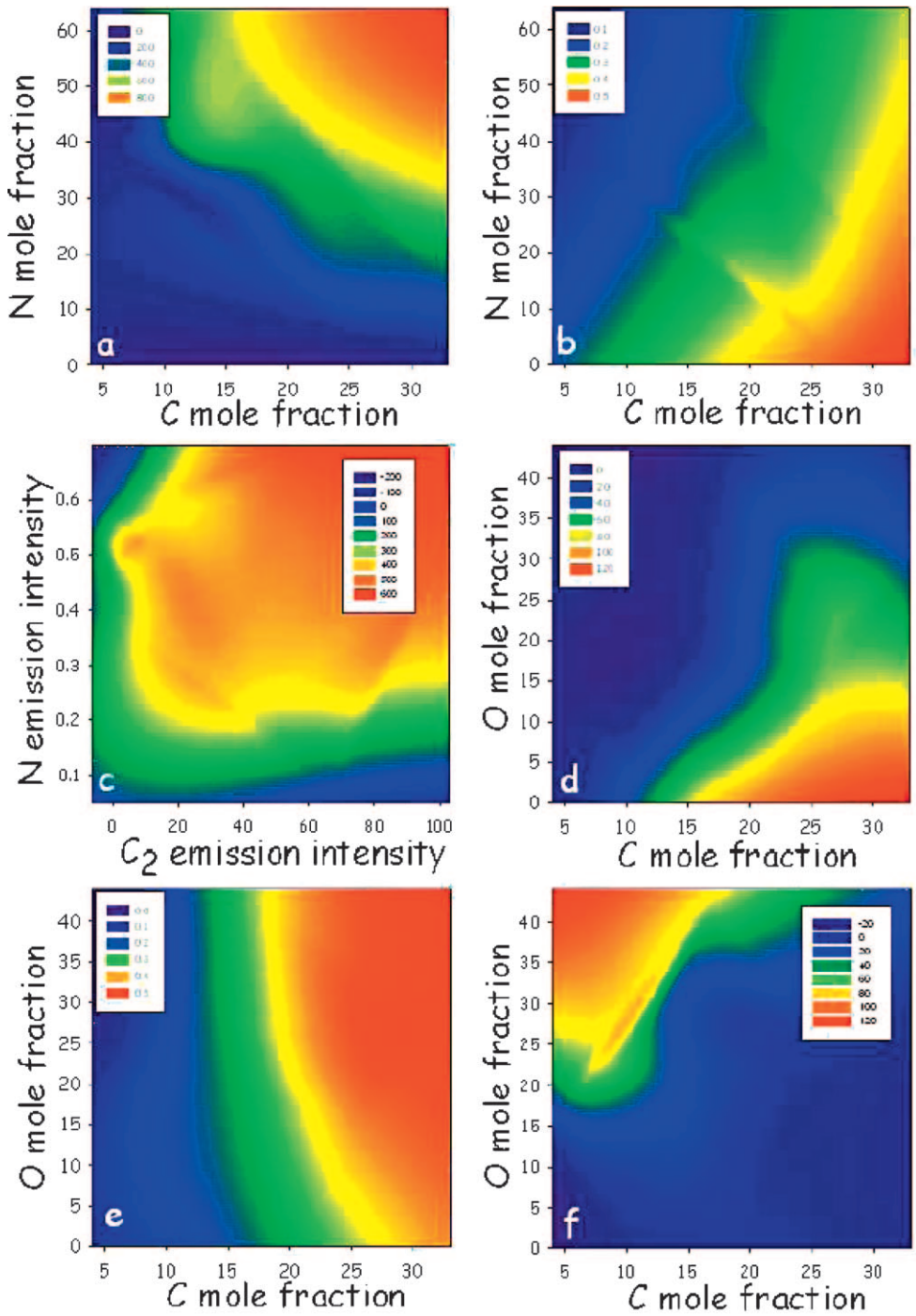

Figure 7. Contour plots created of a) CN intensity against the nitrogen and carbon mole fraction, b) the atomic carbon emission intensity against the nitrogen and carbon mole fraction, c) the CN emission intensity against the nitrogen and C_2 emission intensity, d) the C_2 intensity against the oxygen and carbon mole fraction, e) the atomic carbon emission intensity against the oxygen and carbon mole fraction, and f) the AlO emission intensity against the oxygen and carbon mole fraction.

describe ~90% of the variance. In Figure 9, we show the scores plot of the three principal components.

There are distinct groupings for the majority of the compounds. However, there are some exceptions. H_2bta and HBT overlap since the two compounds are almost identical; the HBT has one extra hydrogen atom and one extra nitrogen atom. The TNT, L-glutamine, sucrose, and, to some extent, melamine are separated due to their high carbon content relative to the other compounds. TNT is separated from these compounds due to its higher oxygen content and, in the case of TNT and sugar, the nitrogen content in TNT. The BTHC is easily separated due to its high oxygen content. The HAT-NO_3 displays interesting behavior in that it appears to have two separate clusters. The two distinct

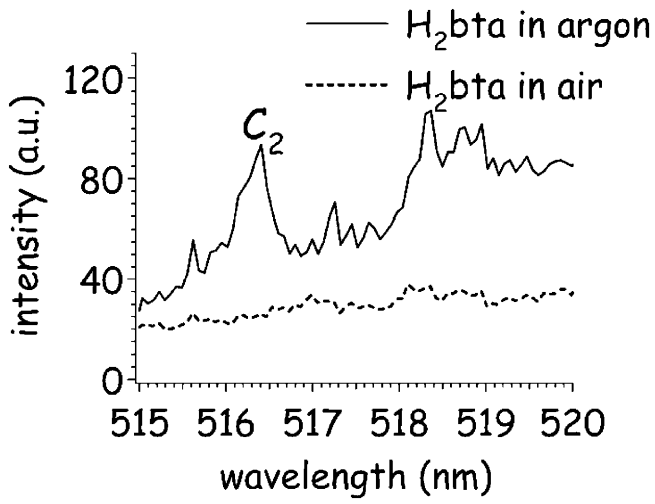

Figure 8. C_2 molecular emission from LIBS spectra of H_2bta in two different bath gases

groupings are from spectra collected on different days. If we compare the normalized carbon, hydrogen, nitrogen, and oxygen values from the HAT-NO_3 collected on different days, we observe that the hydrogen and oxygen have increased in the samples that sat for several days, possibly an indication of water absorption from the air. Thus, several of the atomic emission ratios are different from day to day and the separation occurs in the scores plot. None of the other spectra from compounds collected on different days display this behavior.

4 Conclusion

We have collected and characterized LIBS spectra of a series of nitrogen-containing organic compounds, as well as sucrose. The atomic emission intensities of the constituent elements C, H, N, and O were normalized and used to calculate ratios. These normalized intensities and ratios were then shown to correlate with the mole fraction and the stoichiometric ratio with each respective compound. We also observed the emission from molecular fragments. It has been observed that emission from the molecular fragments CN and C_2 is influenced by the chemical composition of the molecule. As the oxygen mole fraction increases the emission from C_2 decreases because of the formation of CO (and ultimately CO_2). The formation of these molecular fragments also influences the atomic emission from the constituent elements. The increased formation of CN decreases the emission from the atomic carbon line at 247 nm. Despite these effects, the relative intensities from atomic and molecular emissions from a particular compound are strongly correlated to the actual chemical composition. The results from using the ratios and intensities as inputs into the PCA model demonstrate that LIBS can separate these compounds based on just a few key emission lines from the constituent elements.

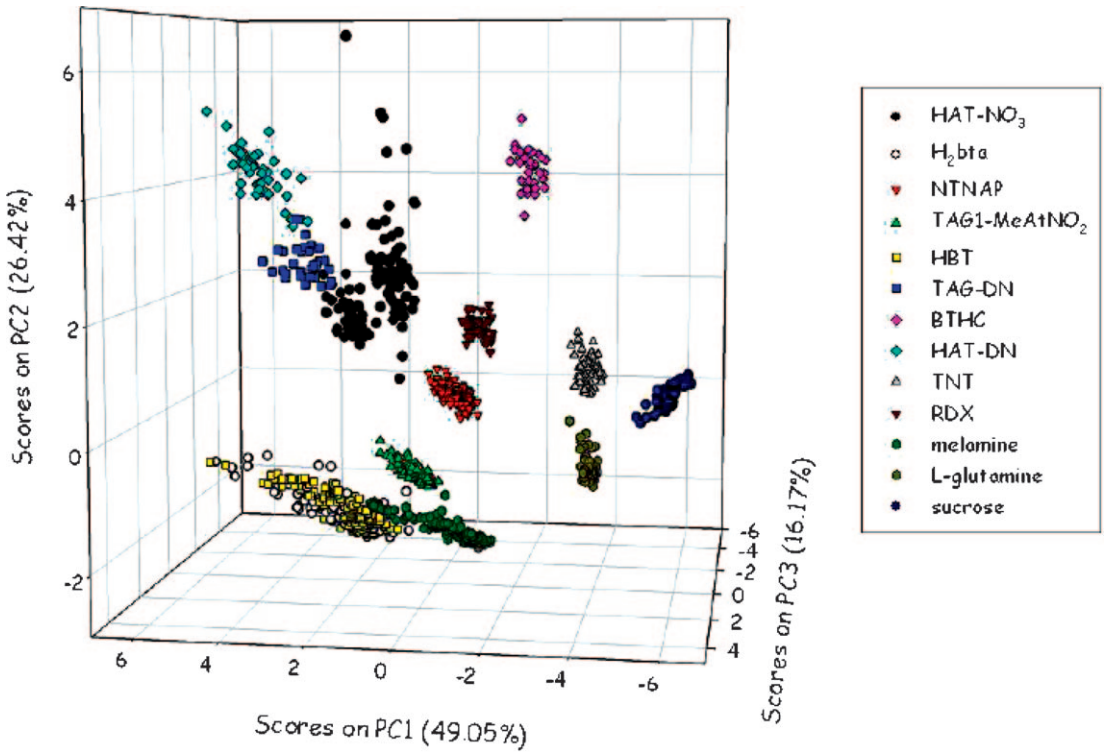

Figure 9. Scores plot of the first three principal components, accounting for $<92\%$ of the total variance from atomic emission intensities and ratios obtained from single shot LIBS spectra of each organic compound.

5 References

[1] T. M. Klapötke, New Nitrogen-Rich High Explosives, in: T. M. Klapötke (Ed.) *High Energy Density Materials*, Springer-Verlag, Berlin Heidelberg **2007**, p. 85.
[2] G. Steinhauser, T. M. Klapötke, "Green" Pyrotechnics: A Chemists' Challenge, *Angew. Chem., Int. Ed.* **2008**, *47*, 3330.
[3] T. M. Klapötke, *High Energy Density Materials*, Springer-Verlag, Berlin Heidelberg **2007**, p. 125.
[4] D. A. Cremers, L. J. Radziemski, *Handbook of Laser-Induced Breakdown Spectroscopy*, John Wiley & Sons, Ltd., West Sussex, England **2006**.
[5] D. A. Rusak, B. C. Castle, B. W. Smith, J. D. Winefordner, Fundamentals and Applications of Laser-Induced Breakdown Spectroscopy, *Crit. Rev. Anal. Chem.* **1997**, *27*, 257.
[6] K. Song, Y. I. Lee, J. Sneddon, Applications of Laser-Induced Breakdown Spectrometry, *Appl. Spectrosc. Rev.* **1997**, *32*, 183.
[7] D. A. Rusak, B. C. Castle, B. W. Smith, J. D. Winefordner, Recent Trends and the Future of Laser-Induced Plasma Spectroscopy, *TrAC, Trends Anal. Chem.* **1998**, *17*, 453.
[8] J. Sneddon, Y. I. Lee, Novel and Recent Applications of Elemental Determination by Laser-Induced Breakdown Spectrometry, *Anal. Lett.* **1999**, *32*, 2143.
[9] J. D. Winefordner, I. B. Gornushkin, D. Pappas, O. I. Matveev, B. W. Smith, Novel Uses of Lasers in Atomic Spectroscopy, *J. Anal. At. Spectrom.* **2000**, *15*, 1161.
[10] J. D. Winefordner, I. B. Gornushkin, T. Correll, E. Gibb, B. W. Smith, N. Omenetto, Comparing Several Atomic Spectrometric Methods to the Super Stars: Special Emphasis on Laser Induced Breakdown Spectrometry, LIBS, a Future Super Star, *J. Anal. At. Spectrom.* **2004**, *19*, 1061.
[11] A. Miziolek, V. Palleschi, I. Schechter, *Laser Induced Breakdown Spectroscopy*, Cambridge University Press, Cambridge, UK **2006**.
[12] C. Pasquini, J. Cortez, L. M. C. Silva, F. B. Gonzaga, Laser Induced Breakdown Spectroscopy, *J. Braz. Chem. Soc.* **2007**, *18*, 463.
[13] J. L. Gottfried, F. C. De Lucia Jr, C. A. Munson, A. W. Miziolek, Laser-Induced Breakdown Spectroscopy for Detection of Explosives Residues: A Review of Recent Advances, Challenges, and Future Prospects, *Anal. Bioanal. Chem.* **2009**, *395*, 283.
[14] F. C. DeLucia Jr., A. C. Samuels, R. S. Harmon, R. A. Walters, K. L. McNesby, A. LaPointe, R. J. Winkel Jr., A. W. Miziolek, Laser-Induced Breakdown Spectroscopy (LIBS): A Promising Versatile Chemical Sensor Technology for Hazardous Material Detection, *IEEE Sens. J.* **2005**, *5*, 681.
[15] M. Tran, S. Sun, B. W. Smith, J. D. Winefordner, Determination of C:H:O:N Ratios in Solid Organic Compounds by Laser-Induced Plasma Spectroscopy, *J. Anal. At. Spectrom.* **2001**, *16*, 628.
[16] F. C. DeLucia Jr., R. S. Harmon, K. L. McNesby, R. J. Winkel Jr., A. W. Miziolek, Laser-Induced Breakdown Spectroscopy Analysis of Energetic Materials, *Appl. Opt.* **2003**, *42*, 6148.
[17] F. C. De Lucia Jr., J. L. Gottfried, C. A. Munson, A. W. Miziolek, Double Pulse Laser-Induced Breakdown Spectroscopy of Explosives: Initial Study Towards Improved Discrimination, *Spectrochim. Acta, Part B* **2007**, *62*, 1399.
[18] J. L. Gottfried, F. C. De Lucia Jr., C. A. Munson, A. W. Miziolek, Strategies for Residue Explosives Detection Using Laser-Induced Breakdown Spectroscopy, *J. Anal. At. Spectrom.* **2008**, *23*, 205.
[19] F. C. De Lucia Jr, J. L. Gottfried, C. A. Munson, A. W. Miziolek, Multivariate Analysis of Standoff Laser-Induced Breakdown Spectroscopy Spectra for Classification of Explosive-Containing Residues, *Appl. Opt.* **2008**, *47*, G112.
[20] J. L. Gottfried, F. C. De Lucia Jr, A. W. Miziolek, Discrimination of Explosive Residues on Organic and Inorganic Substrates Using Laser-Induced Breakdown Spectroscopy, *J. Anal. At. Spectrom.* **2009**, *24*, 288.
[21] M. von Denffer, T. M. Klapötke, G. Kramer, G. Spiess, J. M. Welch, G. Heeb, Improved Synthesis and X-Ray Structure of 5-Aminotetrazolium Nitrate, *Propellants, Explos., Pyrotech.* **2005**, *30*, 191.
[22] T. M. Klapötke, P. Mayer, J. Stierstorfer, J. J. Weigand, Bistetrazolylamines-Synthesis and Characterization, *J. Mater. Chem.* **2008**, *18*, 5248.
[23] R. Boese, T. M. Klapötke, P. Mayer, V. Verma, Synthesis and Characterization of 1-azido-2-nitro-2-azapropane and 1-nitrotetrazolato-2-nitro-2-azapropane, *Propellants, Explos., Pyrotech.* **2006**, *31*, 263.
[24] T. M. Klapötke, J. Stierstorfer, A. U. Wallek, Nitrogen-Rich Salts of 1-Methyl-5-Nitriminotetrazolate: An Auspicious Class of Thermally Stable Energetic Materials, *Chem. Mater.* **2008**, *20*, 4519.
[25] T. M. Klapötke, P. Mayer, C. Miro Sabaté, J. M. Welch, N. Wiegand, Simple, Nitrogen-Rich, Energetic Salts of 5-Nitrotetrazole, *Inorg. Chem.* **2008**, *47*, 6014.
[26] T. M. Klapötke, C. M. Sabaté, Bistetrazoles: Nitrogen-Rich, High-Performing, Insensitive Energetic Compounds, *Chem. Mater.* **2008**, *20*, 3629.
[27] T. M. Klapötke, J. Stierstorfer, Triaminoguanidinium Dinitramide – Calculations, Synthesis and Characterization of a Promising Energetic Compound, *Phys. Chem. Chem. Phys.* **2008**, *10*, 4340.
[28] T. M. Klapötke, J. Stierstorfer, Azidoformamidinium and 5-aminotetrazolium Dinitramide – Two Highly Energetic Isomers with a Balanced Oxygen Content, *Dalton Trans.* **2009**, 643.
[29] M. Göbel, T. M. Klapötke, Replacement of TNT: BTHC, An Insensitive Melt Castable Explosive with Positive Oxygen Balance, *12th Seminar New Trends in Research of Energetic Materials*, Pardubice, Czech Republic, April 1–3, **2009**, p. 548.
[30] L. St-Onge, R. Sing, S. Béchard, M. Sabsabi, Carbon Emissions Following 1.064 μm Laser Ablation of Graphite and Organic Samples in Ambient Air, *Appl. Phys. A* **1999**, *69*, S913.
[31] V. I. Babushok, F. C. DeLucia, P. J. Dagdigian, J. L. Gottfried, C. A. Munson, M. J. Nusca, A. W. Miziolek, Kinetic Modeling Study of the Laser-Induced Plasma Plume of Cyclotrimethylenetrinitramine (RDX), *Spectrochim. Acta, Part B* **2007**, *62B*, 1321.
[32] Y. Song, J.-H. Wu, Y.-P. Wang, G.-D. Wu, X.-D. Yang, Optical Investigation of Shock-Produced Chemical Products in Pseudo-Aluminized Explosive Powders Explosion, *J. Phys. D* **2007**, *40*, 3541.

Acknowledgements

We would like to thank Dr. Brad Forch for introducing us to the high nitrogen molecules developed by Prof. Dr. Thomas Klapötke. We would also like to thank Dr. Rose Ann Pesce-Rodriguez for providing the high nitrogen samples as well as discussions about the chemical composition.

